

PANORAMIC SURVEY OF Ly α EMITTERS AT $z = 3.1$

T. YAMADA¹, Y. NAKAMURA¹, Y. MATSUDA², T. HAYASHINO³, R. YAMAUCHI³, N. MORIMOTO¹, K. KOUSAI³, AND M. UMEMURA⁴

¹ Astronomical Institute, Tohoku University, Aramaki, Aoba-ku, Sendai, Miyagi 980-8578, Japan; yamada@astr.tohoku.ac.jp

² Department of Physics, Durham University, South Road, Durham DH1 3LE, UK

³ Research Center for Neutrino Science, Graduate School of Science, Tohoku University, Sendai 980-8578, Japan

⁴ Center for Computational Physics, University of Tsukuba, Tsukuba, Ibaraki 305, Japan

Received 2010 November 25; accepted 2011 December 1; published 2012 February 24

ABSTRACT

We present the results of the extensive narrowband survey of Ly α emission-line objects at $z = 3.1$ in the 1.38 deg^2 area surrounding the high-density region of star-forming galaxies at $z = 3.09$ in the SSA22 field, as well as in the 1.04 deg^2 area of the three separated general blank fields. In total, of 2161 Ly α emitters, there are 1394 in the SSA22 fields and 767 in the general fields detected at the narrowband AB magnitude limit of 25.73, which corresponds to the line flux of $\approx 1.8 \times 10^{-17} \text{ erg s}^{-1} \text{ cm}^{-2}$ or the luminosity of $\approx 1.5 \times 10^{42} \text{ erg s}^{-1}$ at $z = 3.1$, above the observed equivalent-width threshold, $\approx 190 \text{ \AA}$. The average surface number density of the emitters at $z = 3.1$ in the general fields above the thresholds is $0.20 \pm 0.01 \text{ arcmin}^{-2}$. The SSA22 high-density region at $z = 3.09$, whose peak local density is six times that of the average, is found to be the most prominent outstanding structure in the whole surveyed area and is firmly identified as a robust “protocluster.” We also compared the overdensity of the 100 arcmin^2 and 700 arcmin^2 areas which contain the protocluster with the expected fluctuation of the dark matter as well as those of the model galaxies in cosmological simulations. We found that the peak height values of the overdensity are 8–10 and 3–4 times the expected standard deviations for the counts of Ly α emitters at $z = 3.1$ in the corresponding volume, respectively. We conclude that the structure at $z = 3.09$ in the SSA22 field is a very significant and rare density peak up to the scale of $\approx 60 \text{ Mpc}$.

Key words: galaxies: clusters: individual (SSA22) – galaxies: evolution – galaxies: formation – galaxies: high-redshift – galaxies: starburst – large-scale structure of Universe

Online-only material: color figures

1. INTRODUCTION

Ly α emission from high-redshift galaxies is an important and useful probe in studying the star formation and structure formation history of the universe (Partridge & Peebles 1967). The sensitive narrowband imaging observations have succeeded to detect a large number of the Ly α emitters at intermediate and high redshift toward $z \sim 7$ (e.g., Hu & McMahon 1996; Steidel et al. 2000; Rhoads & Malhotra 2001; Rhoads et al. 2003; Kodaira et al. 2003; Palunas et al. 2004; Hayashino et al. 2004; Matsuda et al. 2004, 2010, 2011; Taniguchi et al. 2005; Gronwall et al. 2007; Iye et al. 2006; Ouchi et al. 2008, 2010).

As the narrowband imaging can constrain the redshift of the objects to the small range, Ly α emitters are also useful in studying the spatial distribution of the star-forming galaxies at high redshift. It is known that high-redshift galaxies are strongly clustered due to the formation bias to the underlying mass distribution (Kauffmann et al. 1999; Benson et al. 2001; Weinberg et al. 2004). While it is not trivial that Ly α emitters follow the simple halo-mass bias in the hierarchical structure formation, since the origins and timescale of the Ly α emission may be diverse, the high-density region of the Ly α emitters may mark the region where galaxy formation preferentially occurs at the epoch. Typical spectral resolution $\delta\lambda/\lambda$ of the narrowband imaging is 50–100, which corresponds to the comoving scale of 50–100 Mpc at $z \sim 3$, and narrow enough to locate the clustered regions and voids.

More than a few high-density regions of the Ly α emitters and star-forming galaxies at high redshift have been studied (Keel et al. 1999; Steidel et al. 2000, 2005; Shimasaku et al. 2003; Palunas et al. 2004; Hayashino et al. 2004; Matsuda et al. 2004, 2009, 2010; Ouchi et al. 2005; Kajisawa et al. 2006; Miley et al. 2006; Venemans et al. 2007; Hatch et al. 2008, 2009;

Overzier et al. 2008; Digby-North et al. 2010; Kuiper et al. 2010; Yang et al. 2010). Among them, the structure at $z = 3.09$ in the SSA22 region, specifically the area around the original selected survey area at 22^h (Cowie et al. 1990), is one of the most prominent and interesting ones. The large density excess was first discovered in the redshift distribution of the Lyman break galaxies (LBGs) by Steidel et al. (1998). The density of the region within $20 \times 15 \times 21 \text{ Mpc}^3$ (in the flat Λ CDM with $H_0 = 70 \text{ km s}^{-1} \text{ Mpc}^{-1}$) comoving volume was reported to be six times greater than that of the average. In fact, the peak has the largest density enhancement in the entire survey volume (Adelberger et al. 1998; Steidel et al. 2003) and it remains one of the largest density peaks discovered at high redshift so far. Subsequent narrowband observations (Steidel et al. 2000; Hayashino et al. 2004; Matsuda et al. 2004) found that the Ly α emitters, which have some overlap with LBGs but are clearly from a different sample in terms of the UV luminosity and the Ly α equivalent width, also show similar density enhancement. The following multiwavelength studies of the field show that the density of the active galactic nuclei (AGNs) detected in X-ray as well as the infrared or submillimeter sources is also high compared to other fields (Geach et al. 2005, 2007; Lehmer et al. 2009; Webb et al. 2009; Tamura et al. 2009).

While the region is often referred to as a “protocluster,” there is still uncertainty regarding the value of the density enhancement of the Ly α emitters as a distinguished structure. First, neither LBGs nor Ly α emitters show prominent concentration on the sky and their distributions extend over the observed fields of view (FoV) of either Steidel et al. (1998) or of Steidel et al. (2000), although some local density structure is recognized (Steidel et al. 2000). Hayashino et al. (2004) revealed that the region is a part of a “belt-like” large-scale structure with the comoving scale of ~ 30 –50 Mpc, which also extends over

Table 1
Summary of the Observed Objects

Field	R.A. J2000.0	Decl. J2000.0	Filter	FWHM (arcsec)	5σ Limit AB mag.	Exp. Time (hr)
SSA22-Sb1	22:17:34.0	+00:17:01.0	<i>N</i> B497	1.0	26.33	7.0
			<i>B</i>	1.0	26.49	1.5
			<i>V</i>	1.0	26.69	1.5
SSA22-Sb2	22:16:36.7	+00:36:52.0	<i>N</i> B497	1.0	26.25	5.5
			<i>B</i>	1.0	26.53	1.0
			<i>V</i>	1.0	26.36	1.0
SSA22-Sb3	22:18:36.3	+00:36:52.0	<i>N</i> B497	1.0	26.30	5.5
			<i>B</i>	1.0	26.81	1.0
			<i>V</i>	1.0	26.55	1.0
SSA22-Sb4	22:19:40.0	+00:17:00.0	<i>N</i> B497	1.1	25.85	5.5
			<i>B</i>	1.1	26.31	1.0
			<i>V</i>	1.1	26.21	1.1
SSA22-Sb5	22:15:28.0	+00:17:00.0	<i>N</i> B497	1.0	26.11	5.5
			<i>B</i>	1.0	26.45	1.0
			<i>V</i>	1.0	26.37	1.0
SSA22-Sb6	22:14:30.7	+00:33:52.0	<i>N</i> B497	1.0	26.27	5.5
			<i>B</i>	1.0	26.83	1.3
			<i>V</i>	1.0	26.58	1.3
SSA22-Sb7	22:17:42.7	+00:56:52.0	<i>N</i> B497	1.0	26.15	5.5
			<i>B</i>	1.0	26.62	1.0
			<i>V</i>	1.0	26.44	1.0
SDF	13:24:39.0	+27:29:26.0	<i>N</i> B497	1.0	26.53	7.2
			<i>B</i>	1.0	27.82	9.9
			<i>V</i>	1.0	27.25	5.7
SXDS-N	02:18:00.0	−05:25:00.0	<i>N</i> B497	1.0	26.19	4.9
			<i>B</i>	1.0	27.56	5.5
			<i>V</i>	1.0	27.08	1.4
SXDS-C	02:18:00.0	−05:00:00.0	<i>N</i> B497	1.0	26.28	5.3
			<i>B</i>	1.0	27.51	5.8
			<i>V</i>	1.0	27.29	1.6
SXDS-S	02:18:00.0	−05:00:00.0	<i>N</i> B497	1.0	26.28	4.8
			<i>B</i> ^b	1.0	27.60	5.5
			<i>V</i> ^b	1.0	27.24	1.8
GOODS-N	12:37:23.6	+62:11:31.0	<i>N</i> B497	1.1	26.55	10.0
			<i>B</i>	1.1	26.68	2.3
			<i>V</i>	1.1	26.15	1.0

the observed field of the Subaru Suprime-Cam, $\approx 27' \times 34'$. While the subsequent spectroscopic observation revealed that this large-scale high-density structure seems to consist of the filamentary structures in the redshift space and the density peak discovered by Steidel et al. (2000) located near the intersection of the filaments (Matsuda et al. 2005), further observations covering the larger area are needed to characterize the density peak in the large volume. The control sample should also be improved. When Steidel et al. (2000) evaluated the density enhancement of Ly α emitters, the compared “field” sample was comprised of those obtained earlier in a relatively small volume (Cowie & Hu 1998; Pascalelle et al. 1996, 1998). Hayashino et al. (2004) referred to the sample they obtained in a general field of area similar to SSA22-Sb1. The data were, however, shallower than that obtained at the SSA22 field and the significance of the overdensity was evaluated by using only the relatively bright objects. A single field for the control sample is also not enough to evaluate the field-to-field variation of the number density of the emitters.

In this paper, we present the results of our wide-field and deep surveys of the Ly α emitters at $z = 3.1$ around the dense structure in the SSA22 fields (Steidel et al. 1998, 2000; Adelberger et al. 1998; Hayashino et al. 2004) as well as the general blank deep survey fields. The survey volume is significantly

enlarged to be 10 times larger than that in Hayashino et al. (2004). The goal of this paper is to characterize the high-density region of the Ly α emitters and to evaluate the significance of their density enhancement. The detection of the extended Ly α nebulae, namely Ly α blobs in the same fields, was reported in our previous paper (Matsuda et al. 2011).

2. DATA

2.1. Observations

We conducted the deep and wide-field imaging observations with the Subaru 8.2 m telescope equipped with the Subaru Prime Focus Camera (Suprime-Cam; Miyazaki et al. 2002). The custom narrowband filter *N*B497 (Hayashino et al. 2004), whose central wavelength and width are 4977 Å and 77 Å, respectively, was used to sample the Ly α emitters at $z = 3.09$. The width corresponds to the redshift range $z = 3.062$ –3.125, or 59 Mpc in the comoving scale.

In order to expand the $z = 3.1$ Ly α emitter survey around the SSA22 region, we first observed the six adjacent Suprime-Cam FoVs around the original field, SSA22-Sb1 (Hayashino et al. 2004; Matsuda et al. 2004). The coordinates of the fields, referred to as SSA22-Sb2 to SSA22-Sb7, and the summary of the observations are shown in Table 1. Their configuration in

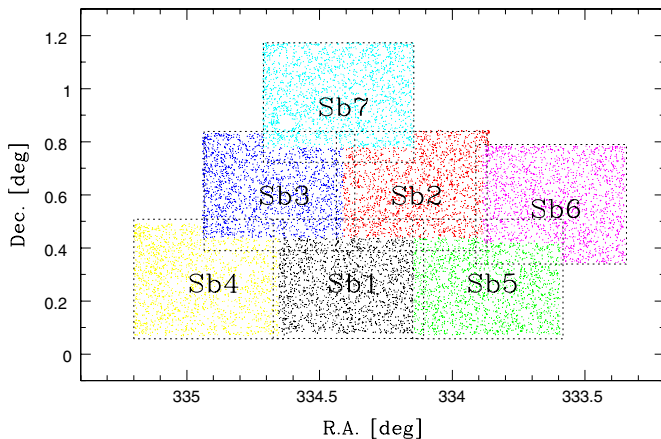


Figure 1. Observed Suprime-Cam fields of view of the SSA22 fields. The boundary used for the analysis in this paper is shown by the colors of the dots which are the $NB497$ -detected objects sampled with a rate of 1 in 50.

the sky is shown in Figure 1. The boundaries of the fields used in this paper are indicated by the colors of the dots which show the positions of the detected sources (1 in 50 of the objects are plotted). Typical exposure time for the $NB497$, B -, and V -band filters are 5 hr, 1 hr, and 1 hr, respectively. The seeing conditions were fairly homogeneous except for some observations of the SSA22-Sb4 field where we need to apply a slight aperture correction to match the other data (see below).

For the control sample, we also obtained the similar deep narrowband data in the five general blank fields, specifically the Subaru/*XMM-Newton* Deep Survey (SXDS)-North, -Center, -South (Furusawa et al. 2008), the Subaru Deep Field (SDF; Kashikawa et al. 2004), and the field around the Great Observatory Optical Deep Survey North (GOODS-N; Dickinson et al. 2004) fields. We also used the broadband data of the SXDS and SDF fields taken and published by each of the other deep survey teams. As the available public broadband data of the Suprime-Cam in the GOODS-N fields are not as homogeneous as the other general fields, we must be careful when analyzing the equivalent-width distribution of the GOODS-N field. Here we simply omitted it in the discussion of the equivalent width.

Thus, in this paper, the data for the seven Suprime-Cam fields in the SSA22 region, including the original SSA22-Sb1 field as well as those of the five Suprime-Cam fields in the three separated general blank fields (SXDS-N, -C, and -S, SDF, GOODS-N), are analyzed. The total areas used in the analysis are 1.38 deg^2 for the SSA22 fields and 1.04 deg^2 for the blank fields.

2.2. Data Reduction

The data reduction was done by using SDFRED (Yagi et al. 2002; Ouchi et al. 2004). The basic procedure is the same as described in Hayashino et al. (2004). After subtracting the *bias* by using the mean value of the overscanned data, the frames are flat-fielded by the flat-fielding frames constructed by the night sky images. The instrumental image distortion and the differential atmospheric dispersion were also corrected. Sizes of the point-spread function (PSF) were then measured by the bright stars and the images were smoothed to match the target PSF size. We matched all of the images except for those from SSA22-Sb4 and GOODS-N to the FWHM of $1''.0$. Since some of the images of the SSA22-Sb4 and GOODS-N fields were relatively poor in seeing, we smoothed them out to the FWHM of $1''.1$. The sky background was then subtracted by the standard procedure in

SDFRED. We adopted a box of $72 \text{ pixels} \times 72 \text{ pixels}$ for the local sky subtraction. After masking the bad regions, all of the chip images were properly aligned and median combined. The broadband images were also aligned to the narrowband images. Astrometry was done by using the USNO stars.

The absolute photometric calibration was done by using the spectroscopic standard stars for the $NB497$ images at SSA22-Sb1 (Hayashino et al. 2004) and at the general fields, and by using the Landolt standard stars for the B - and V -band images at SSA22-Sb1. For the other SSA22 fields Sb2–Sb7, we relatively calibrate them to the Sb1 image by using the overlapping area to ensure the relative homogeneity over the whole area. The uncertainty of the absolute photometric calibration is as large as 0.1 mag but the relative one among the SSA22 fields is 0.01 mag or less at the magnitude range $m_{AB} = 25\text{--}26$, which covers the major fraction of the Ly α emitters. Given that the broadband magnitude values listed in the published catalog of SDF and SXDS objects are robust, we also added a small correction ($\sim 0.05\text{--}0.1$ mag) to the absolute zero-point values (after the correction for Galactic extinction as described below) so that the relative calibration between the SSA22 fields and general fields is also accurate enough to make the sample homogeneous. We use the AB magnitude system throughout this paper and refer to the magnitude in the narrow band as “ $NB497$.”

2.3. Photometry and the Galactic Extinction Correction

The sources were detected by using the software SExtractor 2.1.6 (Bertin & Arnouts 1996). The combined image of each field in each filter was analyzed with SExtractor and the pseudo total flux, FLUX AUTO (or MAG AUTO for magnitude), within a $2.5 \times$ Kron radius as well as the flux within a $2''$ diameter circular aperture were obtained for the detected objects. We also analyzed the broadband images together with the narrowband images by using the SExtractor double-image mode and the FLUX AUTO within the Kron aperture, as well as the fixed aperture at the position at which the narrowband-detected sources were obtained. The photometric errors are dominated by the sky background noise and the 5σ limiting magnitude for the $2''$ diameter aperture in each field is shown in Table 1. Sometimes the narrowband-selected objects are too faint to be detected significantly in the continuum image. In calculating and analyzing the colors or the equivalent width of the objects, we will substitute them as the 1σ limiting magnitude for the aperture.

To obtain the appropriate continuum flux to be compared with the narrowband flux, we constructed the weighted “ BV -band” images by summing the B - and V -band images by $(2B + V)/3$. We refer this average magnitude as BV .

The seeing of the SSA22-Sb4 images was relatively poor and we could not match them to the target image size of $1''.0$. As the seeing of the images from the other 10 fields is better, although we match all of the images to the poorest SSA22-Sb4 one, we made a small correction of 0.061, 0.065, 0.070, and 0.069 mag to the aperture magnitudes in B , $NB497$, V , and BV band for the sources in SSA22-Sb4, respectively. These correction values were obtained by comparing the observed and the artificially degraded images of SSA22-Sb1 and confirmed by comparing the sources in the Sb1–Sb4 overlap region. Since the broadband data of the GOODS-N field also have relatively poor image quality, we also smoothed cut all of the GOODS-N-field images to FWHM = $1''.1$ and applied the same aperture corrections as for SSA22-Sb4.

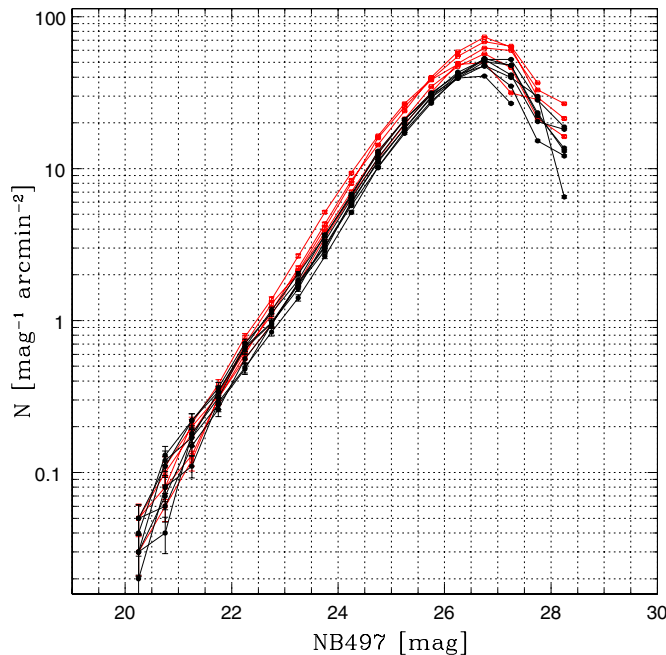


Figure 2. Observed number counts of the sources selected in the $NB497$ images. The data are not corrected for Galactic extinction. The filled circles and black lines show the data for the SSA22 Sb1-Sb7 fields and the open squares and red lines show those for the general fields.

(A color version of this figure is available in the online journal.)

Figure 2 shows the number counts in the $NB497$ band of the detected sources in the SSA22 fields (filled circles and the black lines) as well as for those in the general fields (open squares with the red lines). The counts in the SSA22 fields are systematically low, which is due to the Galactic extinction as the SSA22 fields are located at a relatively low Galactic latitude, $(l, b) \approx (63^\circ, -45^\circ)$. We therefore have to correct the flux of the objects in the SSA22 fields to the Galactic extinction in order to compare the data with the general fields which are located at higher Galactic latitudes. For example, the mean extinction in the V band is 0.22 mag in SSA22 while the mean extinctions are 0.08 mag and 0.06 mag in the SXDS and SDF fields, respectively. The difference of the extinction within the seven SSA22 Suprime-Cam fields should also be carefully considered as we will discuss the inhomogeneity in the spatial distribution of the Ly α emitters over the fields. For that purpose, we refer to the most modern map of Galactic reddening over the sky based on the COBE DIRBE and the IRAS ISSA far-infrared data (Schlegel et al. 1998, hereafter SFD) shown in Figure 3 with the projected seven Suprime-Cam FoVs. The spatial resolution of the SFD map is $0^\circ.32$. The color excess $E(B-V)$ ranges from 0.05 to 0.09, and gradually changes from northwest to southeast.

For all of the detected sources we applied the correction for Galactic extinction from the $E(B-V)$ value at the position of the SFD map by using the following relations, $A_V = 3.16 \times E(B-V)$, $A_B = 4.11 \times E(B-V)$, and $A_{NB497} = 3.55 \times E(B-V)$, based on the extinction curve derived by Kenyon et al. (1994). Figures 4(a) and (b) show the comparison of the source counts between the SSA22 and the general fields as well as those among the seven SSA22 fields after the Galactic extinction correction. While the SFD map smoothed out the patchy structure smaller than $0^\circ.32$, the agreement between the average of the corrected counts in the SSA22 fields and the general fields is reasonably

good. The scatter among the seven SSA22 fields also becomes small after the correction while the field-to-field variation with $\sim 10\%$ in the number density remains. Note that the counts in the SSA22-Sb1 field, shown by the blue line, are the lowest among them and they would not be an artificial cause of the overdensity of the Ly α emitters in the field.

Figure 5 shows the distribution of the $BV - NB497$ colors for the objects between 23 mag and 25 mag in both the bands. The vertical dashed (red) line indicates the peak (mode) value of the SSA22-Sb1 field and the dotted line in each panel shows the same for each field. The peak coincides within ~ 0.02 mag, which enables us to make the uniform selection of the narrowband excess objects.

3. IDENTIFICATION OF THE Ly α EMITTERS

We now describe the selection criteria for the $z = 3.1$ Ly α emitters. The aperture magnitude values are used for this purpose. Figures 6 and 7 show the color-magnitude diagram of the objects detected in the $NB497$ images in the SSA22 fields and in the general fields, respectively. The very slight additional correction for the color zero point left after the photometric calibration above was made in the Ly α emitter (LAE) identification so as to ensure more complete sample homogeneity over the fields.

The criteria to identify the Ly α emitters at $z \sim 3.1$ are as follows.

- (1) $NB497 < 25.73$ ($S/N > 6.6$), and,
- (2a) $BV - NB497 > 1.0$ and $B - V_c > 0.2$
(when $V_c < 26.5$),
or,
- (2b) $BV - NB497 > 1.3$
(when $V_c > 26.5$).

V_c is the line-corrected V -band magnitude. The criteria are similar to those in Hayashino et al. (2004) but the color threshold was slightly relaxed based on the fact that a few contaminations by the foreground objects were found in our previous spectroscopic observations. In fact, the spectroscopic observations (Matsuda et al. 2005, 2006) show that the contamination of the foreground objects, mostly [O II] emitters at $z = 0.33$, is at most 1%, or negligible. The $B - V_c$ criteria are useful to further prevent the contamination of the $z = 0.33$ [O II] emitter, although we cannot apply it to the continuum faint sources, $V_c > 26.5$.

For the robustness of the sample, we also apply an additional constraint that the observed $BV - NB497$ color must be larger than the 4σ value of the background noise in the SSA22-Sb4 field. The limit is shown by the curves in Figures 6 and 7. Only a small fraction of the objects are rejected by the last criteria.

In total, we identified the 1394 and 767 emission-line objects in the SSA22 and blank fields, respectively. The $NB497$ limiting magnitude corresponds to either $\approx 1.8 \times 10^{-17}$ erg s $^{-1}$ cm $^{-2}$ or the luminosity of $\approx 1.5 \times 10^{42}$ erg s $^{-1}$ at $z = 3.09$. The numbers and the area for each field (without overlapping) are summarized in Table 2. Based on the previous studies of SSA22-Sb1, including the spectroscopic observations, we emphasize that the sample is quite robust as the $z = 3.1$ Ly α emitters are not contaminated by the foreground objects by more than $\sim 1\%$ in the fraction. This is also confirmed by the recent spectroscopic data for 100 sources in Sb1 (Yamada et al. 2012) as well as the ongoing observations for Sb2-Sb7 for a few hundred sources. We show the number counts of the $NB497$, B , and V bands of the Ly α emitters in

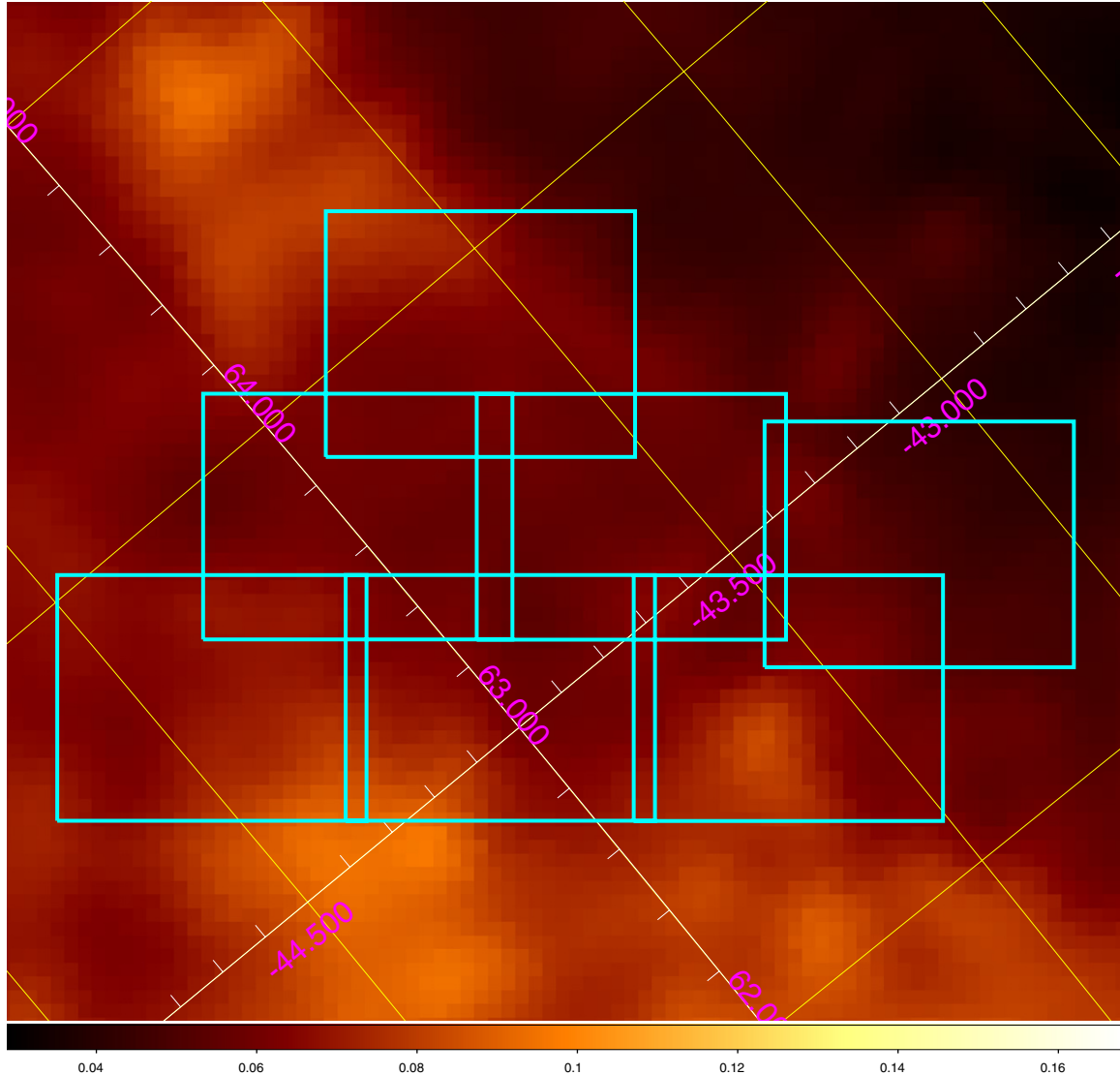


Figure 3. Extinction map converted from the *IRAS* 100 μm data in Schlegel et al. (1998) of the SSA22 fields. The color bar at the bottom shows the $E(B-V)$ value scale. The map is taken from the NASA/IPAC Infrared Service Archive <http://irsa.ipac.caltech.edu/applications/DUST/>. The locations of the SSA22-Sb1 to SSA22-Sb7 fields are shown by the cyan boxes, overplotted by and the Galactic coordinate grid.

Table 2
Numbers of the Detected Ly α Emitters

Field	Area (arcmin ²)	N_{LAE}	Surface Density (arcmin ⁻²)
SSA22-Sb1	647.46	281	0.434
SSA22-Sb2	683.70	166	0.243
SSA22-Sb3	669.29	179	0.267
SSA22-Sb4	750.49	202	0.269
SSA22-Sb5	694.61	201	0.289
SSA22-Sb6	753.14	148	0.197
SSA22-Sb7	781.16	217	0.278
SDF	769.44	196	0.255
SXDS-C	656.31	123	0.187
SXDS-N	697.39	92	0.132
SXDS-S	735.75	171	0.232
GOODS-N	897.16	185	0.206

Figures 8–10. The catalog of the Ly α emitters will be published in a future paper (T. Yamada et al. 2012, in preparation).

4. RESULTS

The sky distributions of the $z = 3.1$ Ly α emitters are shown in Figures 11–14. The separation of 1° corresponds to 109 Mpc in the comoving scale at $z = 3.1$. As shown in Table 2, the surface densities averaged in each Suprime-Cam FoVs of the five blank fields range from 0.13 (SXDS-N) to 0.26 (SDF) arcmin $^{-2}$ and the whole average of the five fields is 0.204 ± 0.007 arcmin $^{-2}$, which corresponds to 1.1×10^{-3} Mpc $^{-3}$.

We also calculated the average densities and the standard deviations for the randomly placed circular areas with various different diameters between 6' and 20'. The average values are nearly constant over the diameters and distribute within the ranges of $0.23\text{--}0.26 \text{ arcmin}^{-2}$ in SDF and $0.16\text{--}0.20 \text{ arcmin}^{-2}$ for the whole SXDS and GOODS-N while the standard deviation decreases as the diameter increases; it is $\approx 0.1 \text{ arcmin}^{-2}$ at the diameter of 6' and $\approx 0.03 \text{ arcmin}^{-2}$ at 20'. In this paper, we adopted 0.20 arcmin^{-2} for the nominal average number density of the Ly α emitters selected by our criteria described above. We also calculated the local smoothed number

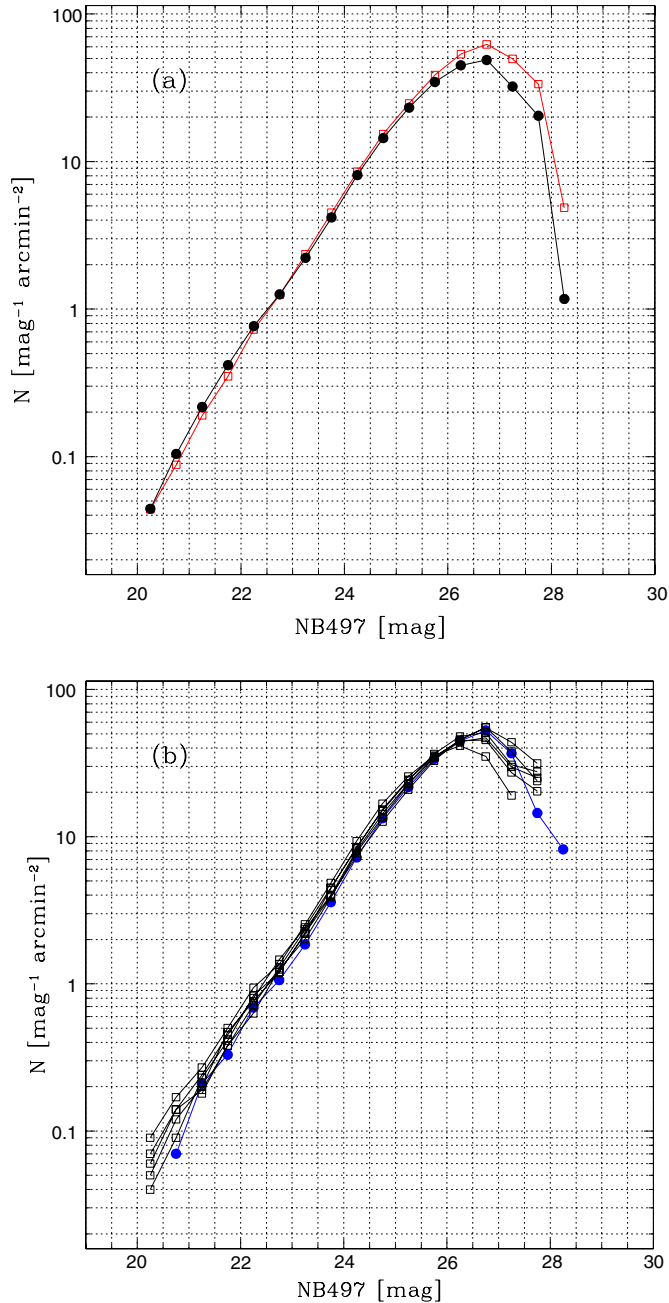


Figure 4. (a) The extinction corrected number counts of the averages of the SSA22 fields (black line and symbols) and the general fields (red one). (b) Same as (a) but those for each of the seven SSA22 fields. The counts of the SSA22-Sb1 field are shown by the blue line. The shallowest data are those of the SSA22-Sb4 field.

(A color version of this figure is available in the online journal.)

density with the Gaussian kernel with $\sigma = 1.5$ and the contours in Figures 11–14 show the smoothed densities of 1.5, 2.5, 3.5, 4.5, and 5.5 times the nominal average density. The large-scale inhomogeneity in the SSA22 is clearly seen in Figure 11 and the number-density excess in the SSA22-Sb1 is evident. The highest peak with ≈ 6 times the average is seen in the SSA22-Sb1 field at $(\alpha, \delta) \approx (334^\circ 35, 0^\circ 3)$, right at the position of the local “peak” discussed in Steidel et al. (2000; northeast one in their Figure 10). There is only one small peak with ~ 3.5 times the average in SDF but none in other general fields. The highest peak in the SSA22-Sb1 is thus very conspicuous.

The densities of the SSA22 Suprime-Cam fields range from 0.20 to 0.44 arcmin^{-2} (Table 2) and the average is 0.28 arcmin^{-2} . The high surface density of the SSA22-Sb1 field is prominent and more than two times higher than the average of the general blank fields. There is also a large under dense region over ≈ 30 Mpc (in the comoving scale) in the eastern half of SSA22-Sb6 at around $(\alpha, \delta) \approx (333^\circ 7, 0^\circ 6)$, while the surface density is high in the western half of SSA22-Sb5 at around $\approx (333^\circ 7, 0^\circ 2)$. The whole average of the SSA22 fields omitting SSA22-Sb1 is 0.25 arcmin^{-2} , which is still higher than the average but a similar value to the SDF, which is the densest among them.

We also compare our results with the previous survey of Ly α emitters at $z \sim 3$. Ouchi et al. (2008) observed the $z = 3.1$ Ly α emitters in SXDS by the slightly different narrowband filter $NB503$ and detected 356 objects in 0.98 deg^2 brighter than $NB503 = 25.3$ and $V - NB503 > 1.2$, which yields a surface number density of $0.099 \pm 0.005 \text{ arcmin}^{-2}$. While the selection criteria are slightly different, we also counted the number of our Ly α emitters with $NB497 < 25.3$ and $BV - NB497 > 1.2$. We found 309 and 530 Ly α emitters in the five general fields (1.04 deg^2) and SSA22 (1.38 deg^2), respectively. The surface density of our sample in the general fields is thus $0.083 \pm 0.004 \text{ arcmin}^{-2}$ which is only slightly smaller than the value in Ouchi et al. (2008). On the other hand, the average surface density in the whole SSA22 field and that in SSA22-Sb1 are 0.11 arcmin^{-2} and 0.18 arcmin^{-2} , respectively, which is similarly high even if we compare the average density of the $NB503$ emitters in Ouchi et al. (2008) to the magnitude and equivalent-width limit.

Gronwall et al. (2007) also searched the Ly α emitters at $z = 3.1$ down to the magnitude limit of ≈ 25.4 and the equivalent-width limit of $\sim 20 \text{ \AA}$ in 0.28 deg^2 and found 167 emitters, or 0.16 arcmin^{-2} . As the width of the narrowband filter is somewhat different (50 \AA in Gronwall et al.), a direct comparison is rather difficult. If we apply the similar selection threshold and corrected the 1.5 times volume difference in a unit area, we found 0.16 arcmin^{-2} for the general fields, and 0.24 and 0.34 arcmin^{-2} in the whole SSA22 and SSA22-Sb1, respectively. Thus, our result is reasonably consistent with the previous results in terms of the number density in the general fields and the very large density excess in the SSA22 fields is robust.

The color–magnitude diagrams of Figures 6 and 7 show that the observed narrowband color excess of the emitters ranges from $BV - NB497 = 1$ (selection limit) to at least 3.5, which corresponds to the equivalent width of the Ly α emission between $\approx 190 \text{ \AA}$ to 1900 \AA in the observer’s frame or $\approx 50 \text{ \AA}$ to 500 \AA in the rest frame at $z = 3.09$. Note that the emission line is located at the shoulder of the V band. If we correct the line flux in the V band, the $BV - NB497$ becomes even larger, especially for the objects with large equivalent widths. The attenuation of the Ly α emissions by the intergalactic medium (IGM) in the line of sight ($\approx 20\%$ at $z = 3$) should also be corrected.

Interestingly, there is a large fraction of objects whose uncorrected rest-frame Ly α equivalent width is larger than $\sim 150 \text{ \AA}$, which corresponds to $BV - NB497 = 2.3$. For a constant continuous star formation model with a 0.05 solar metallicity and Salpeter initial mass function with the upper and lower mass cut of 120 and $0.1 M_\odot$, respectively, the expected equivalent width at an age larger than 10 Myr at the equilibrium phase is $\sim 150 \text{ \AA}$ without any reprocessing of the Ly α and UV flux (Malhotra & Rhoads 2002; Schaerer 2003). If the Ly α emission suffers from

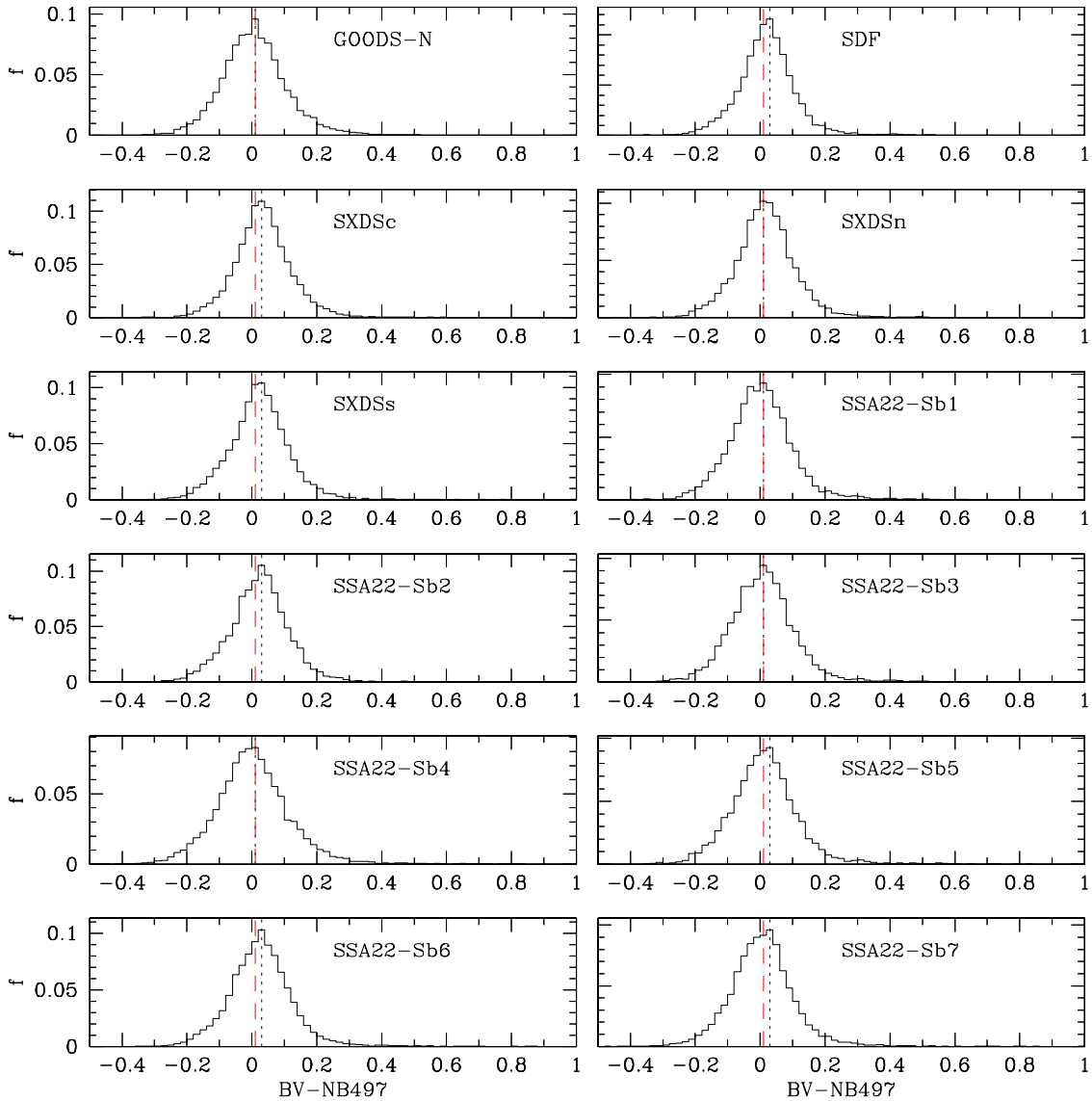


Figure 5. Distribution of the $BV - NB497$ color for the objects between 23 mag and 25 mag in both of the bands.

(A color version of this figure is available in the online journal.)

larger dust extinction due to the large optical path by scattering before escape, this becomes smaller. In the clumpy medium case (Finkelstein et al. 2007), on the other hand, the Ly α equivalent width may be enhanced at most by $\sim 50\%$, and it may be as large as $\sim 230 \text{ \AA}$, which corresponds to $BV - NB497 = 2.7$. The *observed* $BV - NB497$ distribution of our sample spreads over the value. This result suggests that the sample of Ly α emitters is powered by photoionization with hotter stars, namely, younger or metal-poor stars, or by other processes such as the collisional gas heating during the gravitational collapse or galactic superwind.

The distribution of the rest-frame equivalent width calculated from the color measured in $2''$ diameter aperture is shown in Figure 15. Here we corrected for both the V -band line contamination and the attenuation by IGM. We adopted the same value for the IGM attenuation factor, 0.81, as quoted in Ouchi et al. (2008) at $z = 3.1$. The counts in the SSA22 fields from the objects whose BV -band flux is below the detection limit (i.e., only the lower limit of the equivalent width available) are indicated by the light magenta histogram. If we consider

the whole range of the equivalent width, the distribution is not fitted very well by a single exponential law. The best-fitted decaying scale is $112.4 \pm 7.2 \text{ \AA}$ for the whole SSA22 fields and $97.9 \pm 8.7 \text{ \AA}$ for the whole sample of the general fields except for GOODS-N. The fraction of the objects with large equivalent widths is larger in SSA22. On the other hand, if we fit them below 200 \AA , the e -folding value is $73.68 \pm 30.59 \text{ \AA}$ and $63.86 \pm 27.75 \text{ \AA}$, for the SSA22 fields and the general fields, respectively. The larger error is due to the small number of bins. Figure 16 shows the same distribution of the equivalent width but in the cumulative manner. It is more clearly shown that the distribution in the SSA22 fields is more weighted to the larger equivalent-width objects, which is not due to the difference of the detection limit of the continuum bands.

We may also compare the distribution of the equivalent width, although the different continuum depth makes the direct comparison more difficult. Gronwall et al. (2007) found the e -folding scale to be $76+11 - 8 \text{ \AA}$. This is smaller than our results for the full sample of the general fields, $97.9 \pm 8.7 \text{ \AA}$, although they are not very inconsistent considering the errors.

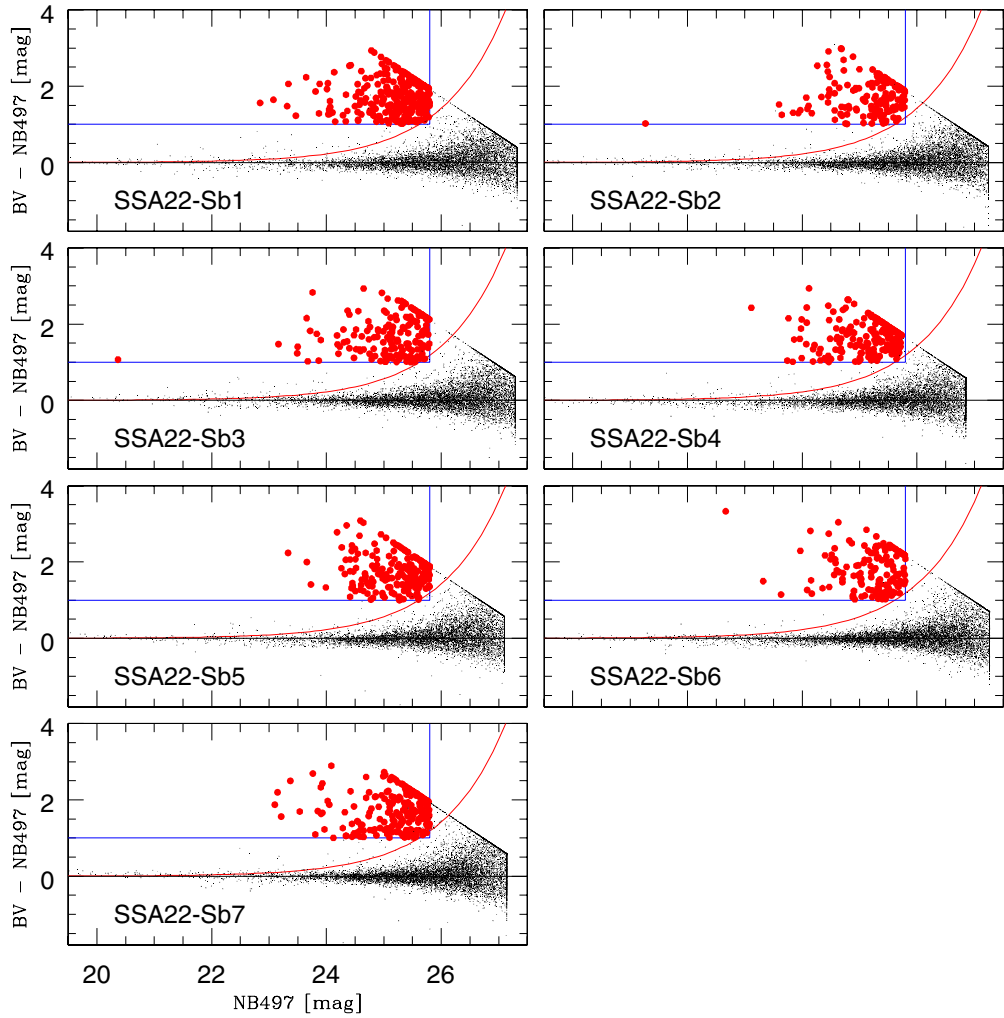


Figure 6. $BV - NB497$ and $NB497$ color magnitude diagram of the SSA22 fields. The BV images are constructed by $(2B+V)/3$. The blue lines show the criteria described in the text. The red curves show the 4σ error of the shallowest SSA22-Sb4 field. While all of the objects that satisfy the criteria are shown by the thick red dots, one-tenth of the other objects are shown by the thin black dots to avoid confusion. The upper bound of the color corresponds to the 1σ detection limit of the BV image.

(A color version of this figure is available in the online journal.)

Since the Ly α emission is typically more extended than the continuum (Hayashino et al. 2004), it may not be appropriate to calculate the equivalent width in the fixed circular aperture when we are interested in the global process in the galaxies for the origins of the Ly α emission. While the fixed aperture should be used to evaluate local processes like photoionization in the star-forming region, the whole extent of the Ly α emission should be considered if we include global scattering effects or other process like shock heating by infalling or outflowing gas. We found that the equivalent width measured in the pseudo total aperture (i.e., SExtractor FLUX AUTO using the Kron aperture) is on average ≈ 1.6 times larger than those measured with the $2''$ diameter apertures. The equivalent-width distribution, which is already spread to the large value above 150 \AA , is further stretched to show the large fraction of the large equivalent-width objects. This trend is seen more conspicuously for the emitters in the SSA22 fields.

5. DISCUSSION

We have constructed a robust and homogeneous sample of the Ly α emitters at $z = 3.1$ around the SSA22 high-density peak as well as the blank fields. The primary result is that the high-

density region originally discovered by Steidel et al. (1998) is now characterized as a very significant structure. It is the most conspicuous density peak in the survey area of a total of 2.42 deg^2 , or in the comoving volume of $1.8 \times 10^6 \text{ Mpc}^3$. No other region shows a density larger than 3.5 times the average of the blank fields. For the number density, the SSA22 high-density region is likely to be rarer than the present-day clusters of galaxies with $L_X(0.5-2 \text{ keV}) \sim 10^{44} \text{ erg s}^{-1}$ (Böhringer et al. 2002), which is about half the luminosity of the Coma cluster.

From Figure 11, the extension of the density peak is $\sim 5 \text{ arcmin} \times 10 \text{ arcmin}$, or $\sim 3 \times 6 \text{ Mpc}$ at $z = 3.1$ in the proper length, if we take the contour of 3.5 times the average as the boundary. The size is comparable with the extension of the X-ray gas of the rich cluster (e.g., $\sim 3 \text{ Mpc}$ for Coma cluster). The overdensity, $\delta N/N_0$, of the Ly α emitter in the region is also found to be very large. The density inside the $\sim 5 \times 10 \text{ arcmin}^2$ area is $\sim 1.0 \text{ arcmin}^{-2}$, which is five times the average density of the general fields, 0.20 arcmin^{-2} . This overdensity is $\approx 10 \times$ the standard deviation of the Ly α emitters in the general field, 0.09 arcmin^{-2} . The structure should correspond to the extremely rare peak which must be a progenitor of the very massive structure if the clustering of the Ly α emitters obey the clustering of

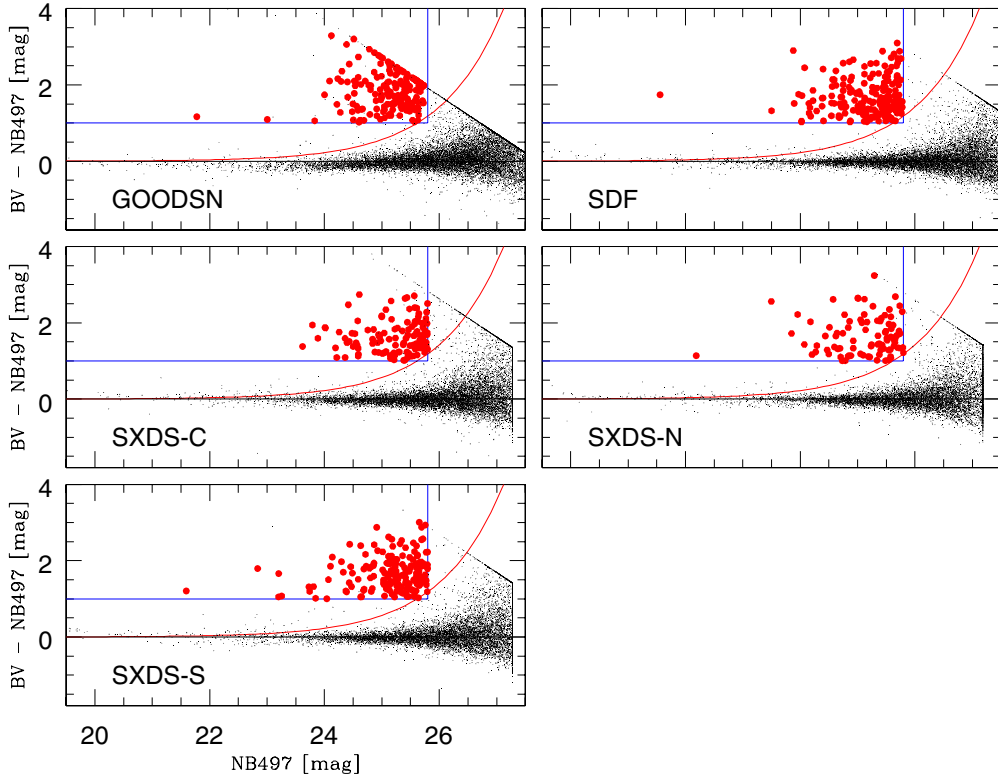


Figure 7. Same as Figure 6 but for the general fields.
(A color version of this figure is available in the online journal.)

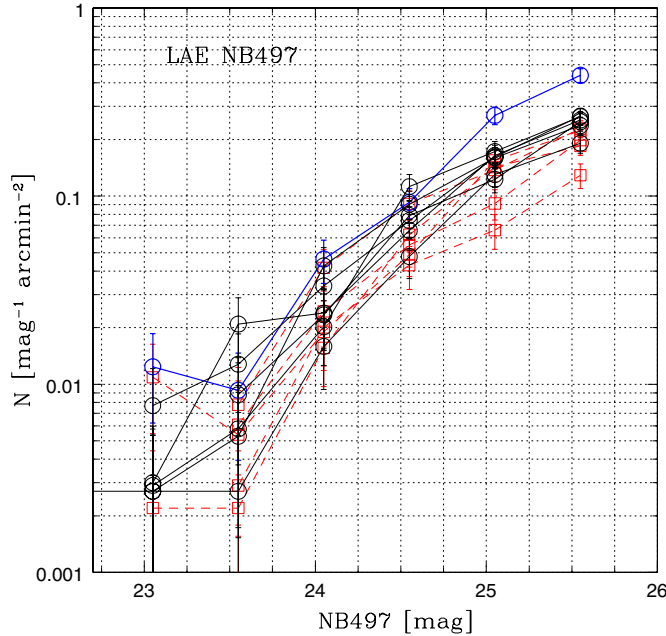


Figure 8. Number counts of the selected Ly α emitters in each field. The blue line with the highest density represents SSA22-Sb1. The five red dashed lines represent the general fields and the black lines represent the other SSA22 fields.
(A color version of this figure is available in the online journal.)

the dark matter halos. Thus, we can confidently call the structure a “protocluster.”

We now evaluate the significance of the overdensity of the high-density region of the Ly α emitters at different scales

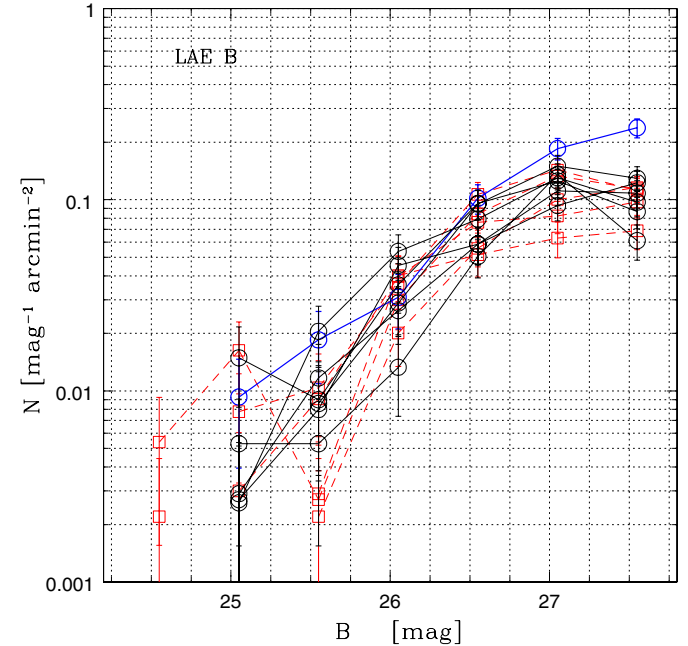


Figure 9. Same as Figure 8 but in the B band.
(A color version of this figure is available in the online journal.)

by comparing them with the predictions for the structure formation models. The area of 700 arcmin^2 , a Suprime-Cam FoV, corresponds to the comoving volume of $1.4 \times 10^5 \text{ Mpc}^3$ for the depth sampled by the narrow band, 59 Mpc. The distribution of the mass or the number-density fluctuation of the galaxies is well approximated by the Gaussian distribution

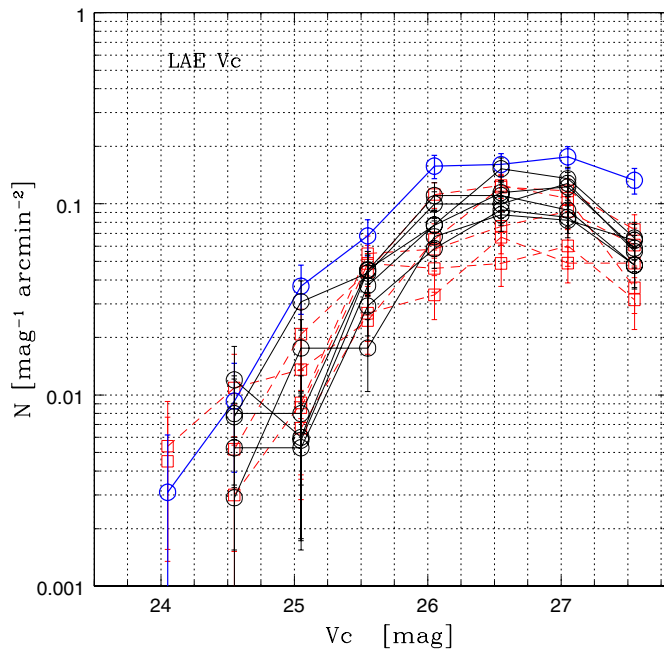


Figure 10. Same as Figure 8 but in the V_c band.

(A color version of this figure is available in the online journal.)

at $z = 3.1$ at this scale. The underlying mass fluctuation can be roughly estimated assuming the standard Λ CDM model with the linear approximation. Adopting the normalization of the power spectrum $\sigma_8 = 0.81$ (Komatsu et al. 2011) and the approximation for the mass variance with the top-hat window, $\sigma(R) = \sigma_8(R/r_8)^{-\beta}$ (Mo et al. 2010) with $\beta \approx 0.7$ (CDM shape parameter $\Gamma = 0.2$), and the linear growth rate in the non-zero cosmological constant (Carroll et al. 1992), ≈ 3.3 at $z = 3.1$, we obtain the $\sigma(R) = \langle (\delta\rho/\rho_0)^2 \rangle^{1/2}$ at the corresponding comoving scale ($R \approx 32$ Mpc) at $z = 3.1$ is ≈ 0.11 . The observed density variation among the five general fields, $(\delta N/N_0)_{\text{LAE}} = -0.38$ (SXDS-N) to $+0.21$ (SDF), is comparable with the value, if we consider that the Ly α emitters trace mass distribution with the linear biasing factor $b \sim 2\text{--}6$, as obtained in the previous study of Ly α emitters at $z = 2\text{--}5$ from the analysis of the two-point correlation functions (Shimasaku et al. 2003; Gawiser et al. 2007; Guaita et al. 2010). On the other hand, the density excess of the SSA22-Sb1 with $(\delta N/N_0)_{\text{LAE}} = 1.13 \pm 0.01$ even at this scale is unexpectedly large, more than $\approx 10\times$ the mass fluctuation, which implies that the field is the very rare, $>5\sigma_{\text{LAE}}$ peak with $b = 2$ (Gawiser et al. 2007).

In Table 3, we also compare the observed overdensity with the expected mass fluctuation for both the smaller area with 100 arcmin^2 that contains the local density peak of the emitters and for the entire seven fields of SSA22. Note that the average density of the general blank fields changes very little with the observed area (Section 3) and it is reasonable to assume the constant average surface density over these scales. The 100 arcmin^2 area centered at $(\alpha, \delta) = (334.392, 0.250)$, which corresponds to the SSA22a in Steidel et al. (2000), contains 89 emitters, which corresponds to the overdensity of 3.36 ± 0.03 while the 1σ mass fluctuation is 0.18. We assumed that the mass fluctuation at this scale was still represented by the $\sigma(R)$ evaluated as above, although the entire distribution may be deviated from the Gaussian at this scale at $z = 3.1$. The peak is confirmed to be very significant, 19 times the average of mass

Table 3
Significance of the Overdensity Compared with Mass Fluctuation

Field	Area (arcmin 2)	N_{LAE}	δ_{LAE}	R_{th}^{a} (Mpc)	σ_{mass}
SSA22 Sb1-Sb7	4980	1394	0.37 ± 0.01	62	0.07
SSA22 Sb1	647	281	1.13 ± 0.01	31	0.11
Sb1 peak	100	89	3.36 ± 0.03	17	0.18

Note. ^a The equivalent radius of the top-hat sphere for the volume.

fluctuation. At the larger scale of the entire SSA22 Sb fields, the overdensity is observed to be 0.37 ± 0.01 while the expected mass fluctuation is 0.07 at this scale. With $b = 2$, it is the 2.6σ peak at the dimension of ≈ 100 Mpc scale. The SSA22 field is a very significant high-density region in the universe on the scale of the Great Wall (Geller & Huchra 1989).

Furthermore, we also compared the overdensity with the distribution of the model galaxies in the cosmological simulation. We use the public semi-analytic model galaxy catalogs at $z = 3.06$ from the Millennium simulation (De Lucia et al. 2006). The distribution of galaxies within the $500 h^{-1}$ Mpc cube and the model parameters for the star formation rate (SFR) and the mass weighted age are available in the catalog. It is not easy to make a sample of the model galaxies that exactly represents the observed Ly α emitters since the Ly α emission may be diverse, not only by the condition of ionization and excitation of the gas, but also by dust extinction and resonance scattering. We chose a sample of star-forming galaxies that may crudely mimic the observed galaxies and investigated their general properties. We first make the samples of the model galaxies by simply dividing by their SFR in order to see how the fluctuation behaves as the SFR of the model galaxies changes. Those with $\text{SFR} > 18 M_\odot \text{ yr}^{-1}$ are in Sample A, $10 M_\odot \text{ yr}^{-1} < \text{SFR} < 18 M_\odot \text{ yr}^{-1}$ are in Sample B, and $6.5 M_\odot \text{ yr}^{-1} < \text{SFR} < 10 M_\odot \text{ yr}^{-1}$ are in Sample C. The ranges are chosen so that the number density is the same as the observed value in the general blank fields. The observed rest-frame ultraviolet continuum flux of the Ly α emitters, $V = 25\text{--}27$ mag, corresponds to the SFR of a few to $\approx 10 M_\odot \text{ yr}^{-1}$ at $z = 3.1$ without reddening correction (Matsuda et al. 2004). Considering that the Ly α luminosity may vary both with the SFR and age, we also make a sample (Sample D) of the model galaxies that satisfy the condition $\log \tau < A/\text{SFR}$, where τ is the age and A is the constant to match their number density to the observed value. Model galaxies, either large SFR or young age, are selected by the criteria.

We then randomly put the boxes which correspond to the 700 arcmin^2 rectangular Suprime-Cam FoV (1000 boxes), or the 100 arcmin^2 square region (5000 boxes), both with a depth of 59 Mpc, into the volume of the Millennium simulation to obtain the distribution of the counts in the boxes. Each distribution is fitted by a single Gaussian function in order to evaluate the standard deviation σ_{model} of the model galaxies in the sample. While the distribution for the 700 arcmin^2 sample can be fitted by the Gaussian function very well from low to high overdensity values, the small tails of the high overdensity are seen for the 100 arcmin^2 samples, especially for Sample A with the large SFR, which can be better represented by the log-normal type probability distribution function. Table 4 summarizes the results. We found that the fluctuation becomes smaller for the sample of the lower SFR, which is reasonable if the objects with higher SFR galaxies are associated with more massive halos on average.

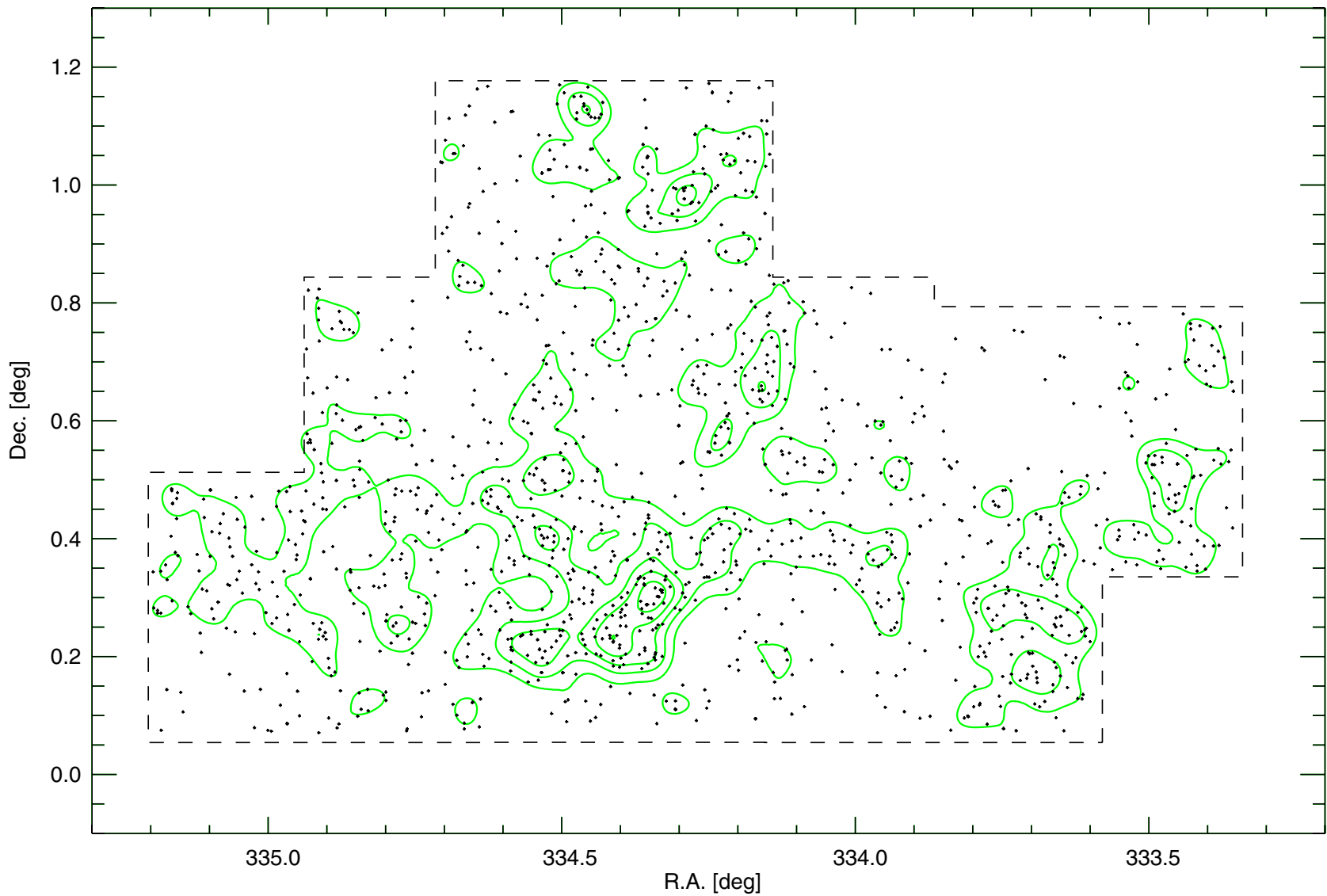


Figure 11. Sky distributions of the Ly α emitters detected in the SSA22 fields.
(A color version of this figure is available in the online journal.)

Table 4
Significance of the Overdensity Compared with the Semi-analytic Model

Sample	SFR Range ($M_{\odot} \text{ yr}^{-1}$)	N_{700}^{a}	σ_{700}^{a}	Peak Height (Sb1)	N_{100}^{b}	σ_{100}^{b}	Peak Height (Peak)
Sample A	>18	144	0.31	3.6	19	0.40	8.4
Sample B	10–18	133	0.27	4.2	18	0.39	8.6
Sample C	6.5–10	151	0.25	4.5	21	0.37	9.1
Sample D	Age SFR	142	0.27	4.2	20	0.40	8.4

Notes.

^a The average numbers and the Gaussian standard deviations for the distribution of the counts in the box that corresponds to the 700 arcmin² area.

^b The average numbers and the Gaussian standard deviations for the distribution of the counts in the box that corresponds to the 100 arcmin² area.

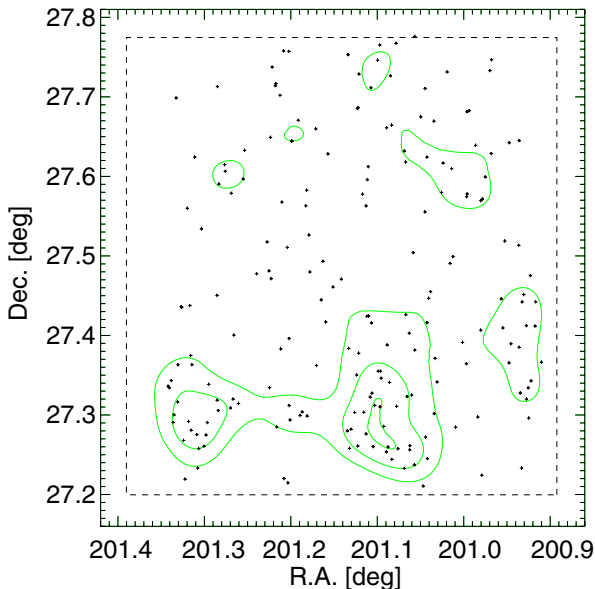


Figure 12. Sky distributions of the Ly α emitters detected in the SDF field.

(A color version of this figure is available in the online journal.)

This trend is small, however, and the standard deviation is not much different among the samples. Compared with these values, the observed overdensity is significantly large, $3.6\text{--}4.5 \sigma_{\text{model}}$ at the 700 arcmin² scale, and $8.4\text{--}9.1 \sigma_{\text{model}}$ at the 100 arcmin² scale.

Thus, we conclude that the high-density region of the SSA22 has a very rare density peak with $3\sigma\text{--}4\sigma$ significance at the scale of ≈ 60 Mpc (diameter), and likely to be $2\sigma\text{--}3\sigma$ at ≈ 100 Mpc. The overdensity is 8–10 times the standard deviation at the ≈ 30 Mpc scale. Note that there is no region with a similar overdensity of the model galaxies in the $(500 h^{-1})^3$ Mpc³ volume of the Millennium simulation in our realizations (1000 boxes and 5000 boxes for the larger and the smaller scales, respectively).

The SSA22 structure is thus characterized as a very important large-scale, high-density region used to study the earliest galaxy formation and evolution in the universe. There is evidence that the active phenomenon related to galaxy formation is enhanced over the large-scale structure. It is important to note that the number density of the giant Ly α blobs with sizes larger than 100 kpc is significantly high in the SSA22 area compared with the other general fields; Matsuda et al. (2010) reported the detection of 12 such giant blobs in the SSA22 fields (in 1.38 deg^2) but only two objects in the general fields (1.04 deg^2).

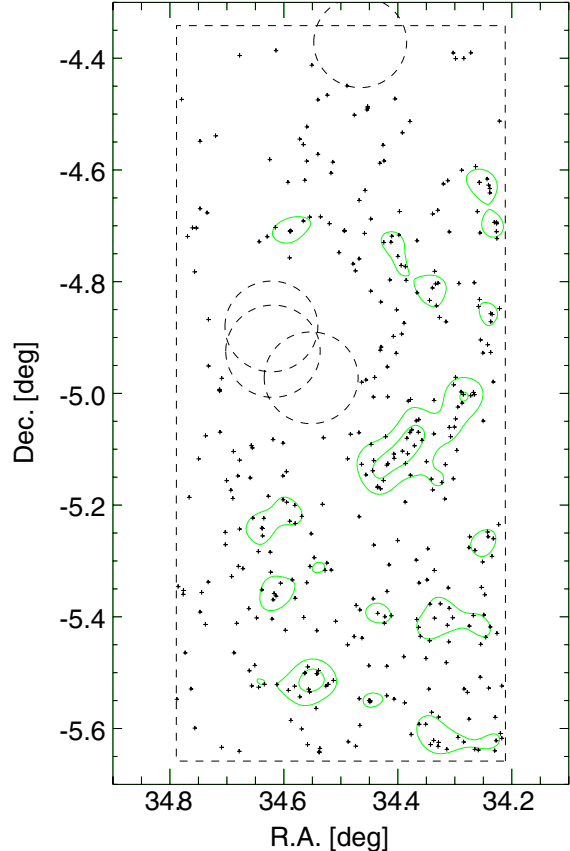


Figure 13. Sky distributions of the Ly α emitters detected in the SXDS fields. The large circles with dashed lines indicate the areas with very bright stars which are omitted from the analysis.

(A color version of this figure is available in the online journal.)

Six objects are distributed in the SSA22-Sb1 field, and of them five are clustered near the density peak of the distribution of Ly α emitters, although they seem to avoid the very central region (see Figure 3 of Matsuda et al. 2010). These giant Ly α blobs are likely to be massive galaxies in their forming phase (Yamada 2009; Uchimoto et al. 2008, 2011). While the formation of the massive galaxies in the densest part might have occurred relatively earlier or faster, as the density peak of the stellar massive objects coincides with that of the Ly α emitters (Uchimoto et al. 2011), it is more active in the surrounding volume at the epoch. Tamura et al. (2009) also reported significant clustering of the bright submillimeter galaxies in the SSA22 field, and they show positive cross-correlation with the sky distribution of the Ly α emitters. Geach et al. (2005,

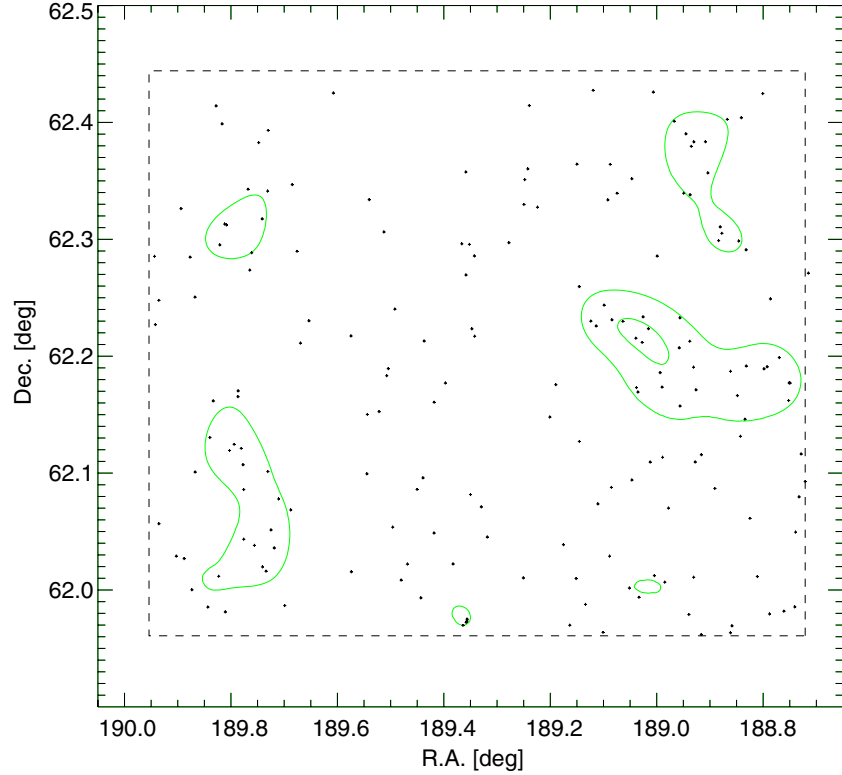


Figure 14. Sky distributions of the Ly α emitters detected in the GOODS-N field.

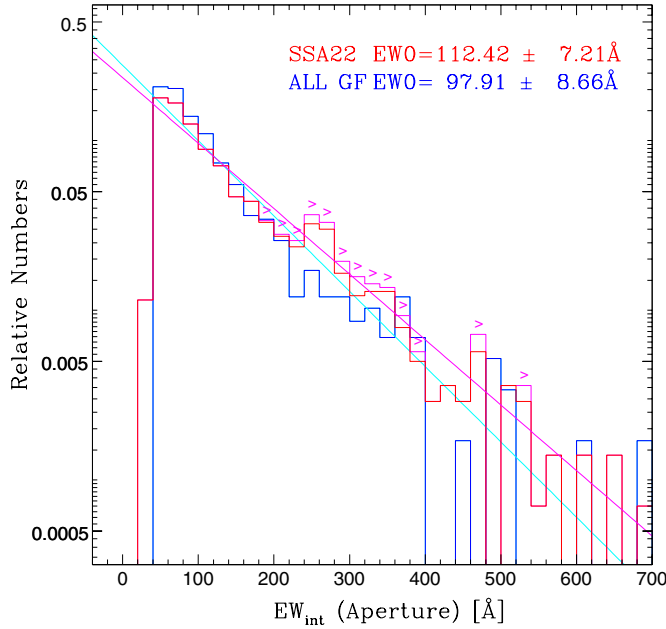


Figure 15. Distributions of the equivalent widths calculated from the 2'' diameter aperture magnitude values. The red histogram is that of the entire SSA22 fields and the magenta lines with “>” show the fraction of the objects whose BV -band continuum is fainter than the upper limit and the obtained equivalent-width values are the only lower limit. The blue histogram is that of the SDF and SXDS fields. The lines are the fitted exponential distribution.

2007) found that more than a few Ly α blobs in Sb1 field are bright submillimeter or infrared sources. Lehmer et al. (2009) and Webb et al. (2009) also show that the fraction of AGNs is also high in the SSA22 field and several Ly α blobs are associated with AGNs. The SSA22 region can be called *the Rosetta Stone*

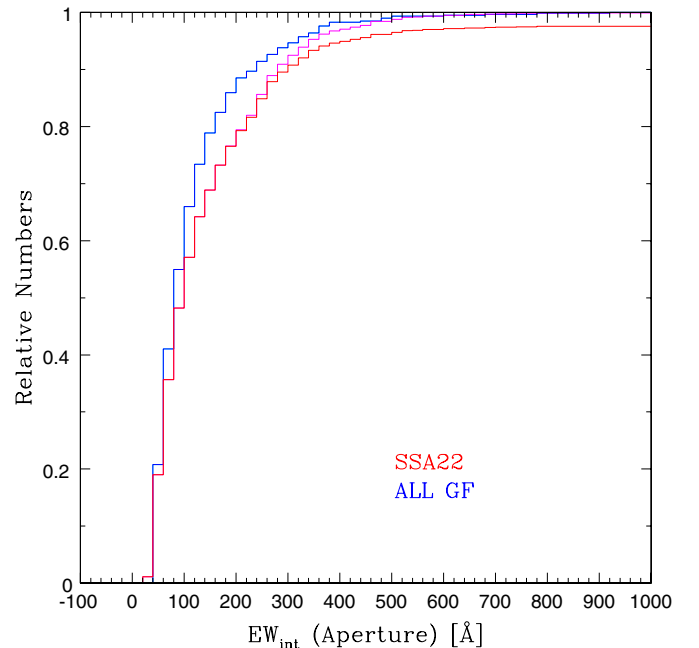


Figure 16. Same as in Figure 15 but presented in the cumulative manner. The magenta line shows the fraction of the lower-limit values of the equivalent width.

because it helps us understand early galaxy formation as a function of the large-scale density of the universe.

We thank the staff of the Subaru Telescope for their assistance. This research is supported in part by the Grant-in-Aid 20450224 for the Scientific Research of the Ministry of Education, Science, Culture, and Sports in Japan. Data analysis was in part carried out on a common use data analysis computer system at the

Astronomy Data Center, ADC, of the National Astronomical Observatory of Japan.

REFERENCES

- Adelberger, K. L., Steidel, C. C., Giavalisco, M., et al. 1998, *ApJ*, **505**, 18
 Benson, A. J., Frenk, C. S., Baugh, C. M., Cole, S., & Lacey, C. G. 2001, *MNRAS*, **327**, 1041
 Bertin, E., & Arnouts, S. 1996, *A&AS*, **117**, 393
 Böhringer, H., Collins, C. A., Guzzo, L., et al. 2002, *ApJ*, **566**, 93
 Carroll, S. M., Press, W. H., & Turner, E. L. 1992, *ARA&A*, **30**, 499
 Cowie, L. L., Gardner, J. P., Lilly, S. J., & McLean, I. 1990, *ApJ*, **360**, L1
 Cowie, L. L., & Hu, E. M. 1998, *AJ*, **115**, 1319
 De Lucia, G., Springel, V., White, S. D. M., Croton, D., & Kauffmann, G. 2006, *MNRAS*, **366**, 499
 Dickinson, M., Stern, D., Giavalisco, M., et al. 2004, *ApJ*, **600**, L99
 Digby-North, J. A., Nandra, K., Laird, E. S., et al. 2010, *MNRAS*, **407**, 846
 Fardal, M. A., Katz, N., Gardner, J. P., et al. 2001, *ApJ*, **562**, 605
 Finkelstein, S. L., Rhoads, J. E., Malhotra, S., Pirzkal, N., & Wang, J. 2007, *ApJ*, **660**, 1023
 Furusawa, H., Kosugi, G., Akiyama, M., et al. 2008, *ApJS*, **176**, 1
 Gawiser, E., Francke, H., Lai, K., et al. 2007, *ApJ*, **671**, 278
 Geach, J. E., Matsuda, Y., Smail, I., et al. 2005, *MNRAS*, **363**, 1398
 Geach, J. E., Smail, I., Chapman, S. C., et al. 2007, *ApJ*, **655**, L9
 Geller, M. J., & Huchra, J. P. 1989, *Science*, **246**, 897
 Goerdt, T., Dekel, A., Sternberg, A., et al. 2010, *MNRAS*, **407**, 613
 Gronwall, C., Ciardullo, R., Hickey, T., et al. 2007, *ApJ*, **667**, 79
 Guaita, L., Gawiser, E., Padilla, N., et al. 2010, *ApJ*, **714**, 255
 Hatch, N. A., Overzier, R. A., Kurk, J. D., et al. 2009, *MNRAS*, **395**, 114
 Hatch, N. A., Overzier, R. A., Röttgering, H. J. A., Kurk, J. D., & Miley, G. K. 2008, *MNRAS*, **383**, 931
 Hayashino, T., Matsuda, Y., Tamura, H., et al. 2004, *AJ*, **128**, 2073
 Hu, E., & McMahon, R. G. 1996, *Nature*, **382**, 281
 Iye, M., Ota, K., Kashikawa, N., et al. 2006, *Nature*, **443**, 186
 Kajisawa, M., Kodama, T., Tanaka, I., Yamada, T., & Bower, R. 2006, *MNRAS*, **371**, 577
 Kashikawa, N., Shimasaku, K., Yasuda, N., et al. 2004, *PASJ*, **56**, 1011
 Kauffmann, G., Colberg, J. M., Diaferio, A., & White, S. D. M. 1999, *MNRAS*, **307**, 529
 Keel, W. C., Cohen, S. H., Windhorst, R. A., & Waddington, I. 1999, *AJ*, **118**, 2547
 Kenyon, S. J., Dobrzycka, D., & Hartmann, L. 1994, *AJ*, **108**, 1872
 Kodaira, K., Taniguchi, Y., Kashikawa, N., et al. 2003, *PASJ*, **55**, L17
 Komatsu, E., Smith, K. M., Dunkley, J., et al. 2011, *ApJS*, **192**, 18
 Kuiper, E., Hatch, N. A., Röttgering, H. J. A., et al. 2010, *MNRAS*, **405**, 969
 Lehmer, B. D., Alexander, D. M., Geach, J. E., et al. 2009, *ApJ*, **691**, 687
 Malhotra, S., & Rhoads, J. E. 2002, *ApJ*, **565**, L71
 Matsuda, Y., Nakamura, Y., Morimoto, N., et al. 2009, *MNRAS*, **400**, L66
 Matsuda, Y., Richard, J., Smail, I., et al. 2010, *MNRAS*, **403**, L54
 Matsuda, Y., Yamada, T., Hayashino, T., Yamauchi, R., & Nakamura, Y. 2006, *ApJ*, **640**, L123
 Matsuda, Y., Yamada, T., Hayashino, T., et al. 2004, *AJ*, **128**, 569
 Matsuda, Y., Yamada, T., Hayashino, T., et al. 2005, *ApJ*, **634**, L125
 Matsuda, Y., Yamada, T., Hayashino, T., et al. 2011, *MNRAS*, **410**, L13
 Miley, G. K., Overzier, R. A., Zirm, A. W., et al. 2006, *ApJ*, **650**, L29
 Miyazaki, S., Komiyama, Y., Sekiguchi, M., et al. 2002, *PASJ*, **54**, 833
 Mo, H., van den Bosch, F. C., & White, S. (ed.) 2010, *Galaxy Formation and Evolution* (Cambridge: Cambridge Univ. Press)
 Ouchi, M., Shimasaku, K., Akiyama, M., et al. 2005, *ApJ*, **620**, L1
 Ouchi, M., Shimasaku, K., Akiyama, M., et al. 2008, *ApJS*, **176**, 301
 Ouchi, M., Shimasaku, K., Furusawa, H., et al. 2010, *ApJ*, **723**, 869
 Ouchi, M., Shimasaku, K., Okamura, S., et al. 2004, *ApJ*, **611**, 660
 Overzier, R. A., Bouwens, R. J., Cross, N. J. G., et al. 2008, *ApJ*, **673**, 143
 Palunas, P., Teplitz, H. I., Francis, P. J., Williger, G. M., & Woodgate, B. E. 2004, *ApJ*, **602**, 545
 Partridge, R. B., & Peebles, P. J. E. 1967, *ApJ*, **147**, 868
 Pascarelle, S. M., Windhorst, R. A., & Keel, W. C. 1998, *AJ*, **116**, 2659
 Pascarelle, S. M., Windhorst, R. A., Keel, W. C., & Odewahn, S. C. 1996, *Nature*, **383**, 45
 Rhoads, J. E., Dey, A., Malhotra, S., et al. 2003, *AJ*, **125**, 1006
 Rhoads, J. E., & Malhotra, S. 2001, *ApJ*, **563**, L5
 Schaerer, D. 2003, *A&A*, **397**, 527
 Schlegel, D. J., Finkbeiner, D. P., & Davis, M. 1998, *ApJ*, **500**, 525
 Shimasaku, K., Ouchi, M., Okamura, S., et al. 2003, *ApJ*, **586**, L111
 Steidel, C. C., Adelberger, K. L., Dickinson, M., et al. 1998, *ApJ*, **492**, 428
 Steidel, C. C., Adelberger, K. L., Shapley, A. E., et al. 2000, *ApJ*, **532**, 170
 Steidel, C. C., Adelberger, K. L., Shapley, A. E., et al. 2003, *ApJ*, **592**, 728
 Steidel, C. C., Adelberger, K. L., Shapley, A. E., et al. 2005, *ApJ*, **626**, 44
 Tamura, Y., Kohno, K., Nakanishi, K., et al. 2009, *Nature*, **459**, 61
 Taniguchi, Y., Ajiki, M., Nagao, T., et al. 2005, *PASJ*, **57**, 165
 Uchimoto, Y. K., Suzuki, R., Tokoku, C., et al. 2008, *PASJ*, **60**, 683
 Uchimoto, Y. K., et al. 2011, *ApJ*, submitted
 Venemans, B. P., Röttgering, H. J. A., Miley, G. K., et al. 2007, *A&A*, **461**, 823
 Webb, T. M. A., Yamada, T., Huang, J.-S., et al. 2009, *ApJ*, **692**, 1561
 Weinberg, D. H., Davé, R., Katz, N., & Hernquist, L. 2004, *ApJ*, **601**, 1
 Yagi, M., Yoshihiko, M., Ogasawara, R., et al. 2002, *Proc. SPIE*, **4847**, 322
 Yamada, T. 2009, *New Astron. Rev.*, **53**, 54
 Yamada, T., et al. 2012, *ApJ*, submitted
 Yang, Y., Zabludoff, A., Eisenstein, D., & Davé, R. 2010, *ApJ*, **719**, 1654